DEFLAGRATION TO DETONATION TRANSITION IN META-STABLE MEDIA

N.N. Smirnov, V.F. Nikitin, J. Khadem, Sh. Alyari Shourekhdeli, V.R. Dushin
Moscow M.V. Lomonosov State University, Leninskie Gory, 1, Moscow 119992, Russia

Propagation of waves in meta-stable systems is sustained by the energy release triggered by the wave front. Combustion waves in chemically reacting systems, and boiling waves in superheated fluids could be considered as typical examples of such self-sustained waves, which could have two modes of propagation: subsonic and supersonic, - due to different mechanisms. The process of transition from one mode of propagation to the other is the most intriguing issue. Investigations of deflagration to detonation transition in gases and pulverized fuel-air mixtures were carried out for pulse detonating devices. The control of detonation onset is of major importance in pulse detonating devices. The advantages of detonation over constant pressure combustion bring to the necessity of promoting the DDT and shortening the pre-detonation length. Most of fuel-air mixtures being heterogeneous the problem of liquid droplet interaction with surrounding gas flow with account of heat and mass transfer and atomization becomes of key interest. The paper contains the results of theoretical investigations of detonation onset peculiarities in homogeneous and polydispersed hydrocarbon–air mixtures. The problem of shock wave initiation of combustible dispersed mixtures is discussed. Mathematical model for liquid droplet interaction with the gas flow is developed with account of non-equilibrium evaporation and atomization. Extensive numerical simulations of droplet thermal and mechanical relaxation in gas flows with account of evaporation and atomization were undertaken and summarized.

Fig.1. Onset of detonation in the flame zone.

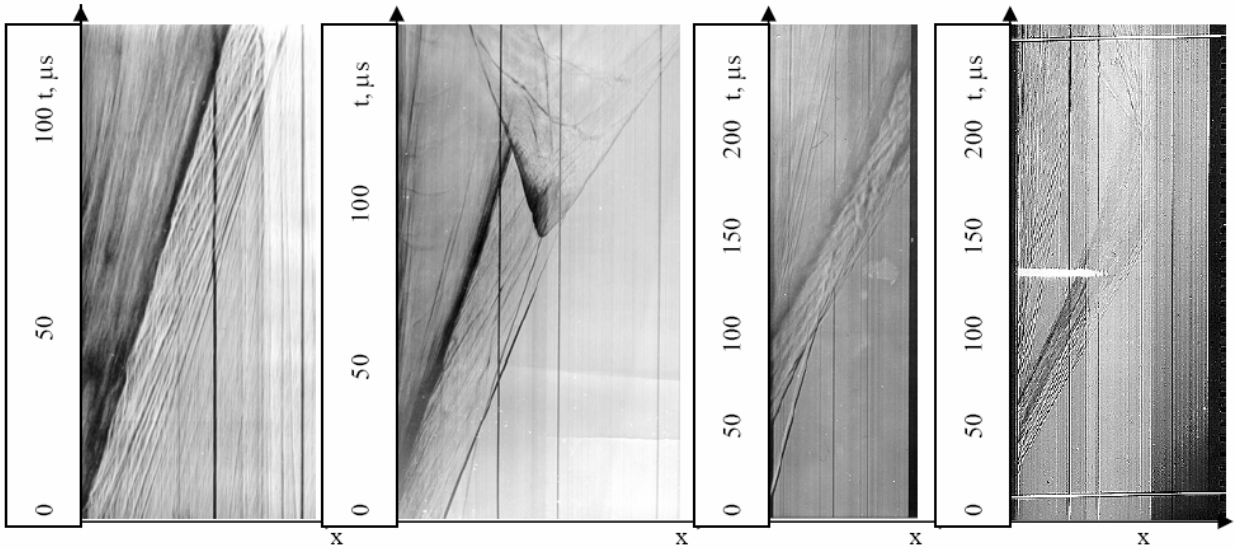

Fig.2. Compression waves ahead of an accelerating turbulent flame.

Fig.3. The onset of detonation ahead of turbulent flame on a contact discontinuity.

Fig.4a. Auto-ignition in a hot spot ahead of the flame giving birth to a new flame zone.

Fig.4b. Auto-ignition in a number of hot spots ahead of the flame

Experimental investigations of the sensitivity of DDT processes to mixture parameters variation have a natural limitation on the precision of the results, because various modes of detonation onset depend on stochastic flow pattern created by accelerating turbulent flames thus making the transition processes non-reproducible in its detailed sequence of events. Figs. 1 - 4 demonstrates schlieren pictures of the detonation onset illustrating different scenarios of DDT in hydrocarbon – air gaseous mixtures. Besides, it is hardly possible to vary different parameters independently

in physical experiments. That increases the importance of numerical modeling for investigating the detonation initiation sensitivity to governing parameters' variations. Numerical investigations of transition processes provide a unique possibility to vary each parameter independently and monotonously.

The paper presents the results of theoretical and experimental investigations of the detonation initiation in homogeneous gaseous and heterogeneous polydispersed mixtures of hydrocarbon fuels with air.

Mathematical model for liquid droplet interaction with the gas flow is developed with account of non-equilibrium evaporation and atomization. The developed mathematical model made it possible taking into account non-equilibrium effects to distinguish two different regimes of droplet evaporation in a heated gas flow: one stage heating and evaporation, and two stages of heating containing a cooling phase in between. Extensive numerical simulations of droplet thermal and mechanical relaxation in gas flows with account of evaporation and atomization were undertaken and summarized. Mathematical models able to predict the onset of detonation in turbulized polydispersed mixtures were developed.

Background.

In 1881 Mallard et Le Chatelier [1] and Bertelot et Vieille [2] were the first to face deflagration to detonation transition process. On investigating flame propagation in homogeneous gaseous mixtures they unexpectedly detected the onset of a supersonic mode of combustion wave traveling at velocities of thousands meters per second. This combustion mode got the name of "false" or "out of tone" combustion, which sounds in French like "detonation" being originated from the French verb "détonner'. The existence of two alternative velocities for the combustion process needed theoretical explanation, which was given in 1993 by an Associate Professor of Moscow University V.A.Mikhelson in his paper " On normal combustion velocity of explosive gaseous mixtures"[3]. Based on having been published by that time papers by Rankine [4] and Hugoniot [5] Mikhelson was the first to explain that the mechanism of flame propagation in detonation was not the heat conductivity, but "adiabatic heating up to the ignition point in shock waves". That was the birth of the classical theory of detonation, which found its further development in the papers by Chapman [6] and Jouget [7].

Investigations of deflagration to detonation transition (DDT) in hydrogen -- oxygen mixtures [8-11] and later in hydrocarbons - air mixtures [12-14] showed the multiplicity of the transition processes scenario. The various modes of the detonation onset were shown to depend on particular flow pattern created by the accelerating flame, thus making the transition process non-reproducible in its detailed sequence of events. By now, there exist different points of view on the DDT mechanism: the "explosion in explosion" mechanism by Oppenheim [9, 11] and the gradient mechanism of "spontaneous flame" by Zeldovich [15].

The later theoretical analysis showed that micro-scale non-uniformities (temperature and concentration gradients) arising in local exothermic centers ("hot spots") ahead of the flame zone could be sufficient for the onset of detonation or normal deflagration [16-22]. Analysis and comparison of theoretical and experimental results showed that self-ignition in one or in a number of hot spots ahead of the accelerating flame followed by the onset of either detonation or deflagration waves brings to a multiplicity of the transition scenarios [23]. The common feature of all those scenarios is the formation of local exothermic centers according to stochastic Oppenheim mechanism followed by the onset of detonation at a micro-scale in one of the exothermic centers according to spontaneous Zeldovich mechanism [23]. The fundamental experimental and theoretical investigations [24, 25] of the reflected shock - laminar flame interactions bringing to the onset of detonation showed, as well, that the transition to detonation in a hot spot takes place through the gradient mechanism, while the shocks and flames interactions were important for creating the proper conditions for the hot spots to occur.

To promote DDT in tubes effective measures were suggested: introducing the Shchelkin spiral in the ignition section [26], incorporating wider turbulizing chambers in the ignition

section (Smirnov's cavities) [12, 23], blocking the initial part of the tube with orifice plates [27]. To bring detonation to a decay detonation arrestors are used [28]. Wider turbulizing chambers were discovered to provide for DDT both promoting effect and inhibiting effect depending on their number and location [29]. The present investigation was aimed at revealing the effects of geometrical characteristics of combustion chambers in flame acceleration and changing the combustion modes.

Mathematical model.

Numerical investigations of the DDT processes were performed using the system of equations for the gaseous phase obtained by Favre averaging of the system of equations for multicomponent multiphase media. The modified *k-epsilon* model was used. To model temperature fluctuations the third equation was added to the *k-epsilon* model to determine the mean squared deviate of temperature [30]. The production and kinetic terms were modeled using the Gaussian quadrature technique.

The mathematical models for simulating turbulent chemically reacting flows in heterogeneous mixtures were described in details in [38, 39]. Combustion processes in heterogeneous mixtures differ greatly from that in homogeneous mixtures, because they are governed not only by chemistry but also by physical processes of combustible mixture formation, such as droplet atomization [40, 41], evaporation and diffusive mixing of fuel vapor with an oxidant.

The model applies both deterministic methods of continuous mechanics of multiphase flows to determine the mean values of parameters of the gaseous phase and stochastic methods to describe the evolution of polydispersed particles in it and fluctuations of parameters. Thus the influence of chaotic pulsations on the rate of energy release and mean values of flow parameters can be estimated. The transport of kinetic energy of turbulent pulsations at the same time obeys the deterministic laws being the macroscopic characteristic.

Averaging by Favre with the $\alpha\rho$ weight , where α – volumetric fraction of the gas phase ($\alpha = 0$ for homogeneous gaseous mixtures), ρ – gas density, we obtain the following system for the gas phase in a multiphase flow [38] (the averaging bars are removed for simplicity):

$$\partial_t(\alpha\rho) + \nabla\cdot(\alpha\rho\vec{u}) = \dot{M} \qquad (1)$$

$$\partial_t(\alpha\rho Y_k) + \nabla\cdot(\alpha\rho\vec{u}Y_k) = -\nabla\cdot\vec{I}_k + \dot{M}_k + \dot{\omega}_k \qquad (2)$$

$$\partial_t(\alpha\rho\vec{u}) + \nabla\cdot(\alpha\rho\vec{u}\otimes\vec{u}) = \alpha\rho\vec{g} - \alpha\nabla p + \nabla\cdot\tau + \dot{\vec{K}} \qquad (3)$$

$$\partial_t(\alpha\rho E) + \nabla\cdot(\alpha\rho\vec{u}E) = \alpha\rho\vec{u}\cdot\vec{g} - \nabla\cdot p\vec{u} - \nabla\cdot\vec{I}_q + \nabla\cdot(\tau\cdot\vec{u}) + \dot{E} \qquad (4)$$

The equations (1-4) include mass balance in the gas phase, mass balance of k-th component, momentum balance and energy balance respectively (p – pressure, $\vec{u}$ – fluid velocity vector, $\vec{g}$ – gravity acceleration vector, E – specific energy, $\dot{\vec{K}}$ – specific momentum flux to gas phase, $\dot{M}$ – specific mass flux, $\dot{E}$ – specific energy flux, τ – turbulent stress tensor). We have the following relationships between the terms in the equations (1-2):

$$\sum_k Y_k = 1 \ , \quad \sum_k \dot{M}_k = \dot{M} \ , \quad \sum_k \vec{I}_k = 0 \ , \quad \sum_k \dot{\omega}_k = 0 \ .$$

The state equations for gaseous mixture are the following:

$$p = R_g\rho T\sum_k Y_k W_k \ , \quad E = \sum_k Y_k(c_{vk}T + h_{0k}) + \frac{\vec{u}^2}{2} + k \ . \qquad (5)$$

where k – turbulent kinetic energy, W_k - molar mass of k-th gas component, h_{0k} – specific chemical energy, c_{pk}, c_{vk} – specific heat capacity. The term responsible for chemical transformations, $\dot{\omega}_k$ is very sensitive to temperature variations, as it is usually the Arrhenius law type function for the reactions' rates. To take into account temperature variations the source term $\dot{\omega}_k$ in the equations (2) was modeled using the Gaussian quadrature technique.

Let us regard the temperature being a stochastic function T with mean $\overline{T}$ and mean squared deviate $\theta = \overline{T'T'}$. Then, the mean value of a function having T as independent variable could be determined as follows:

$$\overline{f(T)} = \int f(\overline{T} + \zeta\sqrt{\theta}) P_d(\zeta) d\zeta,$$

where ζ is a random value with zero expectation and unit deviate; its probability density function is $P_d(\zeta)$. To estimate the integral, the minimal number of terms is used(namely, three) and $P_d(\zeta)$ is assumed to be even. In this case, the formula for *f(T)* averaging is:

$$\overline{f(T)} = \frac{1}{2\chi^2} f(\overline{T} - \chi\sqrt{\theta}) + \left(1 - \frac{1}{\chi^2}\right) f(\overline{T}) + \frac{1}{2\chi^2} f(\overline{T} + \chi\sqrt{\theta}).$$

In case of normal (Gaussian) deviate, the value of χ is equal to $\sqrt{3}$ (Gauss-Hermite case). Therefore, the formula above could be transformed as follows:

$$\overline{f(T)} = \frac{1}{6} f(\overline{T} - \sqrt{3\theta}) + \frac{2}{3} f(\overline{T}) + \frac{1}{6} f(\overline{T} + \sqrt{3\theta}).$$

In our case, the function *f(T)* is the Arrhenius temperature dependence; the whole average for $\dot{\omega}_k$ is constructed using combinations of these dependencies. Averaged magnitudes for mass fractions and density were used in the Arrhenius law for $\dot{\omega}_k$ as the dependence of these functions is not as strong as the dependence of temperature.

The turbulent heat flux $\vec{I}_q$ in the equation (4) is a sum of two terms:

$$\vec{I}_q = \vec{J}_q + \sum_k (c_{pk} T + h_{0k}) \vec{I}_k, \tag{6}$$

where $\vec{J}_q$ could be interpreted as turbulent conductive heat flux. The eddy kinematic viscosity ν^t is expressed according to k-epsilon model as $\nu^t = C_\mu \frac{k^2}{\varepsilon}$. The turbulent fluxes are:

$$\tau = \alpha(\mu + \rho\nu^t)(\nabla\vec{u} + \nabla\vec{u}^T - (2/3)(\nabla\cdot\vec{u})U) - (2/3)\alpha\rho k U, \tag{7}$$

$$\vec{I}_k = -\alpha\rho(D + (\nu^t/\sigma_d))\nabla\cdot Y_k, \tag{8}$$

$$\vec{J}_q = -\alpha(\lambda + \sum_k c_{pk}\rho(\nu^t/\sigma_t))\nabla\cdot T, \tag{9}$$

The model is closed then by the equations for k, θ and ε:

$$\partial_t(\alpha\rho k) + \nabla\cdot(\alpha\rho\vec{u}k) = \nabla\cdot(\alpha(\mu + \rho(\nu^t/\sigma_k))\nabla k) + \tau^t : \nabla\vec{u} - \alpha\rho\varepsilon \tag{10}$$

$$\partial_t(\alpha\rho\varepsilon) + \nabla\cdot(\alpha\rho\vec{u}\varepsilon) = \nabla\cdot(\alpha(\mu + \rho(\nu^t/\sigma_\varepsilon))\nabla\varepsilon) + (\varepsilon/k)(C_{1\varepsilon}\tau^t : \nabla\vec{u} - C_{2\varepsilon}\alpha\rho\varepsilon) \tag{11}$$

$$\partial_t(\alpha\rho\theta) + \nabla\cdot(\alpha\rho\vec{u}\theta) = \nabla\cdot(\alpha(? + \sum_k c_{pk}\rho(\nu^t/\sigma_k))\nabla\theta) + P_\theta + W_\theta - D_\theta, \tag{12}$$

where the production terms P_θ, W_θ and the dissipation term D_θ are:

$$P_\theta = 2\alpha\rho\tilde{c}_p \frac{\nu_t}{\sigma_k}|\nabla T|^2, \; W_\theta = -\sum_k \overline{\omega_k T'} h_{0k}, \quad D_\theta = C_g \alpha\rho \sum_k c_{pk} \frac{\varepsilon}{k} \frac{\theta}{\theta_m - \theta}. \tag{13}$$

The constants take the following values [31, 39, 40]:

$$C_\mu = 0.09, \quad C_{1\varepsilon} = 1.45, \quad C_{2\varepsilon} = 1.92, \quad \sigma_d = 1, \quad \sigma_t = 0.9, \quad \sigma_k = 1, \quad \sigma_\varepsilon = 1.13.$$

$$\theta_m = \overline{T}^2/4. \qquad C_g = 2.8.$$

The gaseous phase was supposed to contain the following set of species: $O_2;\ C_nH_m; CO; CO_2; H_2; H_2O; N_2$.

The chemical potential of hydrocarbon fuel h_2^0 was considered to be a problem parameter, along with its composition *n* and *m*. The potential depends not only on *n* and *m* but also on particular hydrocarbon fractions the fuel consists of. The following brutto reactions between the species were considered:

$$C_nH_m + \left(\frac{n}{2} + \sigma\frac{m}{4}\right)O_2 \to nCO + \sigma\frac{m}{2}H_2O + (1-\sigma)\frac{m}{2}H_2 \quad CO + 0.5O_2 \to CO_2$$

$$CO_2 + M \to CO + 0.5O_2 + M$$

$$H_2 + 0.5O_2 \to H_2O$$

$$H_2O + M \to H_2 + 0.5O_2 + M$$

Here, σ is the share of water in hydrocarbon decomposition. This parameter depends on the particular content of fuel (like the hydrocarbon chemical potential). We denote B=5 - reactions number. The rates of species origination are supposed to yield the Arrhenius law and the acting masses law. With multiple reactions, the origination rates are split into elementary parts:

$$\dot{\omega}_k = \sum_{j=1}^{B} \omega_{kj} \ .$$

where ω_{kj} is the k-th species origination rate per volume due to j-th reaction. The actual formulas for determining ω_{kj} for the present reaction mechanism are described in [30].

Each term ω_{kj} incorporates Arrhenius function for the j-th reaction $A_j(T)$, which is assumed to have the following form:

$$A_j(T) = \begin{Bmatrix} K_j \exp\left(-\frac{T_{aj}}{T}\right), T \ge T_{mj} \\ 0, \qquad\qquad T < T_{mj} \end{Bmatrix}$$

where K_j is the pre-exponential factor, T_{aj} is the activation temperature, T_{mj} is the minimum temperature. In order to obtain the term W_θ (13), one should find the mean values $\overline{T'A_j(T)}$ using formula (11) and then sum those terms up using respective formulas. The procedure for averaging non-linear functions was described in details in [30].

The boundary of the computational domain contains the outer walls and the axis of symmetry. The walls for the case of cylindrical symmetry could be a combination of coaxial cylindrical surfaces and rings or plates orthogonal to the axis. The boundary conditions for the gas phase are constructed in accordance with the following considerations: the walls of the cylindrical domain are thermo-insulated and non-catalytic, the velocity of gas is zero on the walls and the averaged gas motion has cylindrical symmetry.

The boundary conditions for turbulent parameters $k, \quad \varepsilon, \quad \theta$ are constructed according to the wall laws [23]:

$$k = 0, \quad \frac{\partial\varepsilon}{\partial\vec{n}} = 0, \quad \frac{\partial\theta}{\partial\vec{n}} = 0,$$

where $\vec{n}$ is the normal vector to the wall. To take into account the wall damping effect the coefficients of the original turbulence model are modified in accordance with the Lam-Bremhorst low Reynolds models [32]:

$$C_\mu = C_\mu^0 f_\mu,$$
$$C_{1\varepsilon} = C_{1\varepsilon}^0 f_1,$$
$$C_{2\varepsilon} = C_{2\varepsilon}^0 f_2,$$

where f_μ, f_1, f_2 are positive functions: $0 < f_\mu \le 1, f_1 \ge 1, 0 \le f_2 \le 1$, and which depend on two local Reynolds numbers

$$R_t = \frac{k^2}{\nu\varepsilon}, \quad R_y = \sqrt{k}\frac{y}{\nu},$$

where y is a distance from the nearest wall. For the Lam-Bremhorst low Reynolds $k-\varepsilon$ model the functions are determined in the following way:

$$f_\mu = [1-\exp(-0.0165R_y)]^2\left(1+\frac{20.5}{R_t}\right),$$

$$f_1 = 1+\left(\frac{0.05}{f_\mu}\right)^3,$$

$$f_2 = 1-\exp(-R_t^2).$$

The system of gas-dynamics equations being rewritten in a vector form was split in three parts due to three different physical processes: chemistry, source terms, generalized turbulence production terms formed the "local part" of the equations; convective terms formed the "hyperbolic part" of the equations; and diffusive, viscous and thermo-cunductive terms formed the "parabolic part" of the equations.

The local part was solved implicitly using an iterative algorithm independently for each grid node. The hyperbolic part was solved using explicit FCT techniques [33]. The parabolic part was solved implicitly using 3-diagonal matrix solvers for linear equations [34]. The techniques removed viscosity from the time step criterion and reduced it to the Courant-Friedrichs-Lewy criterion.

To solve the system of equations splitting by coordinates was used according to MacCormack [35]. Validation of the numerical scheme was performed by comparing the results of test runs with the exact gas-dynamics solutions and with model experiments on turbulent flames propagation in confined volumes.

The ignition was modeled by energy release in a ball-shape volume at the axis of tube in the center of the first chamber.

One could see that the equations (10-12) do not contain terms responsible for particulate phase contribution to turbulence energy growth. This is due to the direct stochastic modeling of the particulate phase: the influence of the last on the gas phase leads to stochastic behavior of the momentum source terms $\dot{\vec{K}}$. These terms affect the averaged gas phase velocity in the stochastic manner and therefore the source term $\tau^t:\nabla\vec{u}$ is also affected. The motion of polydispersed droplets (particles) is modeled making use of a stochastic approach. A group of representative model particles is distinguished. Motion of these particles is simulated directly taking into account the influence of the mean stream of gas and pulsations of parameters in gas phase [38, 40].

Droplet – gas interaction.

The momentum equation for a single droplet motion in the gas flow has the following form

$$m\frac{d\vec{u}}{dt} = m\vec{g} - \phi\cdot\nabla p + \vec{f}_d, \quad \frac{d\vec{r}}{dt} = \vec{u}, \tag{14}$$

where the drag force could be expressed as follows:

$$\vec{f}_d = \frac{C_d}{2}\rho_g\frac{\pi d^2}{4}(\vec{v}-\vec{u})|\vec{v}-\vec{u}|, \tag{15}$$

the drag coefficient being the function of Reynolds number [43]

$$C_d = \left(\frac{24}{\mathrm{Re}}+\frac{4,4}{\sqrt{\mathrm{Re}}}+0,42\right)\beta\cdot K, \tag{16}$$

$$\mathrm{Re} = \frac{\rho|\vec{v}-\vec{u}|d}{\mu}, \tag{17}$$

$$\beta = \sqrt{\frac{\rho}{\rho_s}\left(2-\frac{\rho}{\rho_s}\right)}, \quad K = \left(\frac{T}{T_s}\right)^{4/5}, \text{ where}$$

$$\frac{\rho_s}{\rho}=\begin{cases}\left(1+\dfrac{\gamma-1}{2}M^2\right)^{1/(\gamma-1)}, & M<1;\\ \dfrac{(\gamma+1)M^2}{(\gamma-1)M^2+2}\left(1+\dfrac{\gamma-1}{2}\cdot\dfrac{(\gamma-1)M^2+2}{2\gamma M^2-(\gamma-1)}\right)^{1/(\gamma-1)}, & M\geq 1.\end{cases} \tag{18}$$

The energy equation for a droplet has the following form

$$m\frac{de}{dt}=q+Q_s\text{, where } e=c_{vs}T_s+h_f^0. \tag{19}$$

The energy of phase transitions could be determined by the formula:

$$Q_s=\frac{dm}{dt}h_L, \tag{20}$$

where h_L is the latent heat of evaporation. Heat flux to a single droplet from the surrounding gas flow is determined as follows [43]

$$q=\begin{cases}\pi d\lambda\cdot\mathrm{Nu}\cdot\left(T-T_s\right), & \mathrm{Re}<1000;\\ \pi d^2\rho\left|\vec{v}-\vec{u}\right|\cdot\mathrm{St}\cdot\left(H_r-H_w\right), & \mathrm{Re}\geq 1000.\end{cases} \tag{21}$$

where

$$\mathrm{Nu}=2+0{,}16\cdot\mathrm{Re}^{2/3}\cdot\mathrm{Pr}^{1/3},\quad \mathrm{St}=\frac{C_d}{2}\mathrm{Pr}^{-2/3}, \tag{22}$$

On reaching by the droplet temperature the boiling value the evaporation rate is determined by a simple formula

$$\frac{dm}{dt}=-\frac{q}{h_L},\quad T=T_b. \tag{23}$$

Else the non-equilibrium evaporation model is used to determine the evaporation rate

$$\dot{m}=\pi d\cdot\rho D\cdot\mathrm{Nu}\cdot\log\left(\frac{1-Y_e}{1-Y_w}\right), \tag{24}$$

$$Y_w=\frac{W_N P_0}{Wp}\exp\left[\frac{H_b}{R}\left(\frac{1}{T_b\left(P_0\right)}-\frac{1}{T_s}\right)\right]-\dot{m}\frac{\sqrt{2\pi RT_s}}{\pi\delta_e pd^2}. \tag{25}$$

The dynamic interaction of liquid droplets with the gaseous flow could bring to instability of the interface and atomization of droplets. The criterion for liquid droplets instability is that of the critical Weber number [41]: $\mathbf{We}=\dfrac{\rho v_{rel}^2 d}{\sigma}$, where σ is the surface tension at the interface, v_{rel} is relative velocity of a droplet versus gas. On exceeding the critical value of the Weber number droplets breakup due to vibrational instability takes place. On essentially surpassing the critical Weber number other mechanisms start playing essential roles in the breakup process that brings to formation of fine mist. These main characteristics of the atomization process could be taken into account by the following approximate formula [39] determining mean diameters of droplets d_a originating in breakups of initial droplets (diameter d):

$$d_a=\begin{cases}d=\left(\dfrac{6\alpha_2}{\pi n}\right)^{1/3}, & \mathbf{We}<\mathbf{We}_*;\\ \dfrac{d\mathbf{We}_*}{\mathbf{We}}, & \mathbf{We}_*\leq\mathbf{We}\leq\mathbf{We}_{**};\\ d_*, & \mathbf{We}>\mathbf{We}_{**};\end{cases} \tag{26}$$

where n is the number of droplets per volume unit, α_2 – volumetric fraction of the droplet phase, the critical Weber numbers are determined as follows:

$$\mathbf{We}_* = 12(1+\mathbf{Lp}^{-0.8}),\ \mathbf{We}_{**} = 350, \tag{27}$$

where the Laplace number $Lp = \dfrac{d\rho_c\sigma}{\mu_c^2}$, ρ_c, μ_c - liquid density and viscosity.

To determine the mean diameter of droplets d_* after the breakup of a type of an explosion ($\mathbf{We} > \mathbf{We}_{**}$) one needs to evaluate the part of the accumulated by a droplet elastic energy spent for the breakup. The assumption, that the breakup energy was spent for the formation of new free surface [40] makes it possible to evaluate the number N and the mean diameter d_* of the formed droplets:

$$N = \left(1+\frac{E_*}{\sigma\pi d^2}\right)^3;\ d_* = \frac{d}{1+\dfrac{E_*}{\sigma\pi d^2}}. \tag{28}$$

The breakup energy could be evaluated as the difference between the work of the drag forces separating small droplets from the initial one, and the kinetic energy of fragments' scattering:

$$E_* = A_{drag} - \sum_{i=1}^{N_*}\frac{m_i v_{i*}^2}{2}. \tag{29}$$

Assuming that the initial droplet is split into N_* equal droplets ($N_* = \dfrac{d^3}{d_*^3}$) having equal velocities of radial expansion of the cloud v_* and the separation of droplets takes place after the droplet is moved away at a distance $\sim d_*$, one obtains the following formulas:

$$A_{drag} = \frac{1}{8}N_*\rho C_d v_{rel}^2\pi d_*^2 d_*;\qquad d_* = \frac{d}{1+\dfrac{1}{4}\left(\dfrac{1}{2}C_d\rho v_{rel}^2 - \dfrac{1}{3}\rho_c v_*^2\right)\dfrac{d}{\sigma}}. \tag{30}$$

The mean velocity of the cloud expansion v_* could be evaluated based on the condition of matching the two formulas for d_a at $\mathbf{We} = \mathbf{We}_{**}$. The reason to perform that matching is that both formulas for breakup regimes were obtained from experiments, thus, indirectly the expansion of the cloud of droplets after the breakup should have been taken into account. On the other hand, the dependence of characteristic droplets diameters on the Weber number should be continuous. Then, finally one obtains

$$d_* = \frac{d\mathbf{We}_*}{\dfrac{1}{8}C_d(\mathbf{We}-\mathbf{We}_{**})\mathbf{We}_* + \mathbf{We}_{**}}. \tag{31}$$

In modeling droplets breakup in a gas flow the inertia of the process should be taken into account. Fragmentation does not take place instantaneously: it needs time for small droplets to separate from the initial one, i. e. it needs a definite time for the liquid bridges between the droplets to be established, elongated and broken [40]. The first order estimate of the breakup time gives the following formula:

$$t_* = \frac{d}{v_{rel}}\frac{\mathbf{We}_*}{\mathbf{We}}\left(1+\frac{3}{8}C_d\frac{\rho}{\rho_c}\left(1-\frac{4}{C_d\mathbf{We}_*}\right)\right). \tag{32}$$

Results of numerical modeling.

Numerical modeling made it possible to explain the scenario of flame acceleration and the onset of detonation on the contact surface ahead of the flame zone. In flame acceleration weak shock waves in gas precede the deflagration wave. The interaction of shock waves gives birth to a rarefaction wave moving backward to the flame front and the contact discontinuity that exists

between the leading shock and the flame zone. The zone between the leading shock and the contact surface has a higher temperature. Thus the induction period in this zone is less than between the flame front and the contact surface. The first thermal explosion takes place in the layer of gas that has been at the higher temperature for the longest time, i.e. in the gas layer on the contact surface. That explosion can bring to either deflagration or detonation waves propagating from the exothermic center. Following the gradient mechanism detonation waves propagating in opposite directions could be formed in this zone. The intensity of the retonation (reverse detonation) wave falls down on entering the reaction products. The detonation wave overtaking the leading shock forms an overdriven detonation in the uncompressed mixture that gradually slows down to the Chapman-Jouget speed.

Experimental investigations of the deflagration to detonation transition in combustible gases testified that the presence of different turbulizing elements in the initial sections of detonation tubes promotes DDT by shortening the pre-detonation length and pre-detonation time. Turbulizing chambers of a wider cross-section were found to be one of the most effective geometrical promoters for the DDT. Numerical experiments were undertaken for comparative studies of the role of different turbulizing elements and their location in the tube. In numerical simulations the test vessel contained a detonation tube with a number of chambers of a wider cross-section incorporated in different places of the tube filled in with combustible gaseous mixture at ambient pressure (Fig. 5). Ignition of mixture was performed by a concentrated energy release in the center of the first chamber or the tube itself in the left hand side near the closed end. The number of chambers was varied from one to twenty. Simulations were performed for the following cases:

1) the initial section had two incorporated turbulizing chambers of a wider cross-section;
2) the far end section had two similar incorporated turbulizing chambers of a wider cross-section;
3) turbulizing chambers were located along the whole tube.

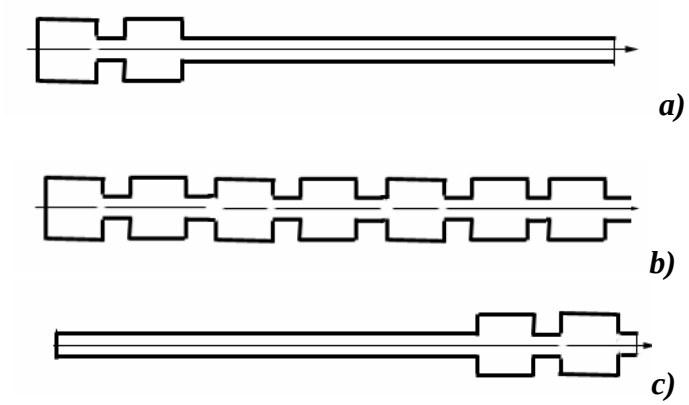

Fig. 5. Geometry of the computational domain.

The role of chambers in the ignition section.

To investigate the influence of turbulizing chambers of a wider cross-section on the onset of detonation numerical modeling was performed for a test vessel containing a detonation tube with two chambers of a wider cross-section (Fig. 5) filled in with combustible gaseous mixture at ambient pressure. Ignition of the mixture was performed by a concentrated energy release in the center of the first chamber. The results show the process of flame propagation that in the first chamber is rather slow and is determined mostly by initial turbulization of the mixture. The flame accelerates and penetrates the bridge between the two chambers due to a gas flow caused by the expansion of reaction products. A high velocity jet penetrating the second chamber brings to a very fast flame propagation both due to additional flow turbulization and the piston effect of the expanding reaction products supported by the continuing combustion in the first chamber Fast combustion in the second chamber brings to a sharp pressure increase that pushes the flame further into the tube, which gives birth to strong flow nonuniformity and shock wave formation in the tube ahead of the flame zone. At some place the detonation arises from a hot spot within

the combustion zone, which gives birth to strong detonation and retonation waves. Fig. 6 shows reaction zone trajectory (left) and mean flame front velocity (right) variation in the tube versus time for the cases of tube incorporating two chambers in the ignition section (Fig. 6,a), and a tube without any chambers (Fig. 6,b). It is seen that the onset of detonation in a tube without chambers is an unstable stochastic process, and each pulsation of velocity depending on some additional disturbance could result in the onset of detonation. The increase of the number of chambers incorporated into the ignition section to one or two makes the DDT more stable and brings to the decrease of pre-detonation length.

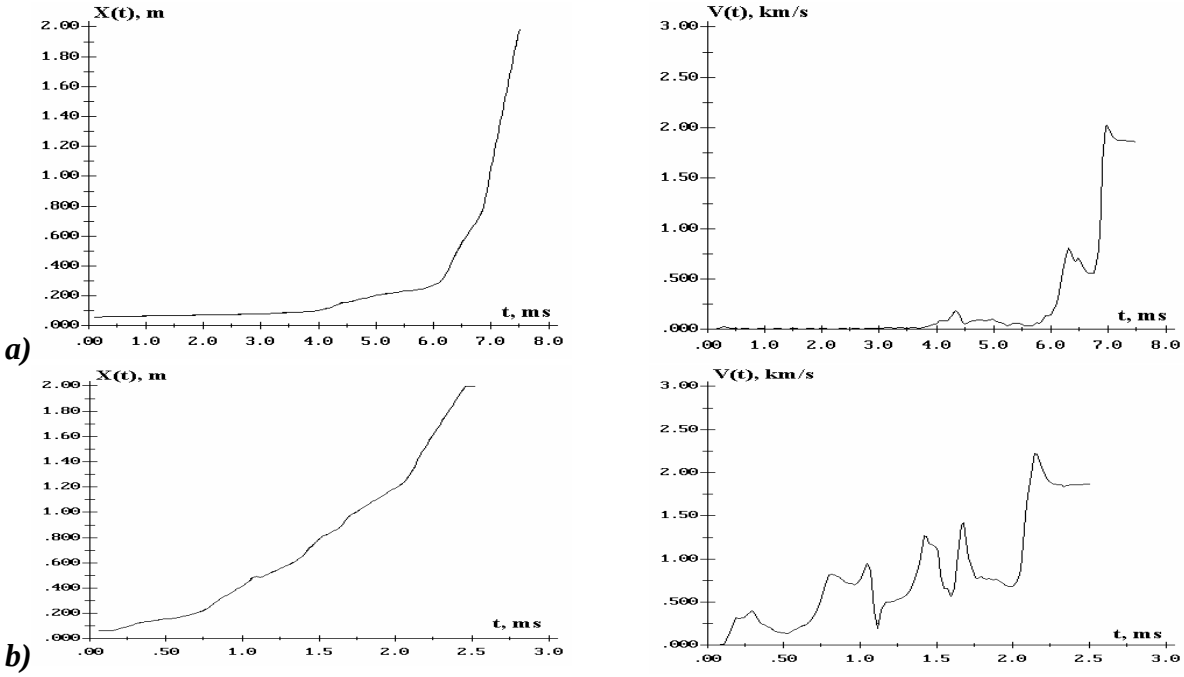

Fig. 6. Reaction zone trajectory (left) and mean flame front velocity (right) variation in the tube versus time for fuel concentration C_{fuel}=0.012: ***a*** **-** tube incorporating two chambers in the ignition section, ***b*** **-** tube without any chambers.

<u>The influence of fuel concentration.</u>

Fig.7 *a-d* shows the corresponding reaction zone trajectory and mean flame front velocity variation in the tube for different values of fuel concentration, but for one and the same tube geometry. Mean flame velocities are also marked for different parts of the trajectories. It is seen that flame accelerates on entering the second chamber, then it slows down. A high speed combustion wave enters the detonation tube, where the transition takes place.

Analysis of results present in Fig.7 shows that on decreasing the fuel content of the mixtures its detonability via DDT decreases. The pre-detonation time increases (Figs.7*a,b*), but once the onset of the detonation takes place it propagates at a practically constant velocity. Velocity diagrams testify, that in both cases the onset of detonation takes place via an overdriven regime.

The decrease of fuel molar concentration below C_{fuel} = 0.011 brings to formation of galloping combustion regimes. Those galloping combustion regimes are not caused by numerical instability as one cycle of the process develops within 150 – 200 time steps. The hot spots occur alternatively near lateral walls (higher pressure pikes) and in the center and bring to flame zone accelerations. The reaction zone trajectories and velocities shown in Fig.7 *c,d* allow to evaluate oscillations. For fuel concentration 0.011 the galloping combustion regime propagates with velocity oscillations within the range of 420 – 1200 m/s. The onset of detonation does not take place within the 2.25 m length of the tube. The average velocity of the galloping combustion mode here was 760 m/s. For fuel concentration 0.010 the galloping combustion begins later and propagates with a lower velocity: oscillations within the range 270 - 1000 m/s, average velocity 435 m/s.

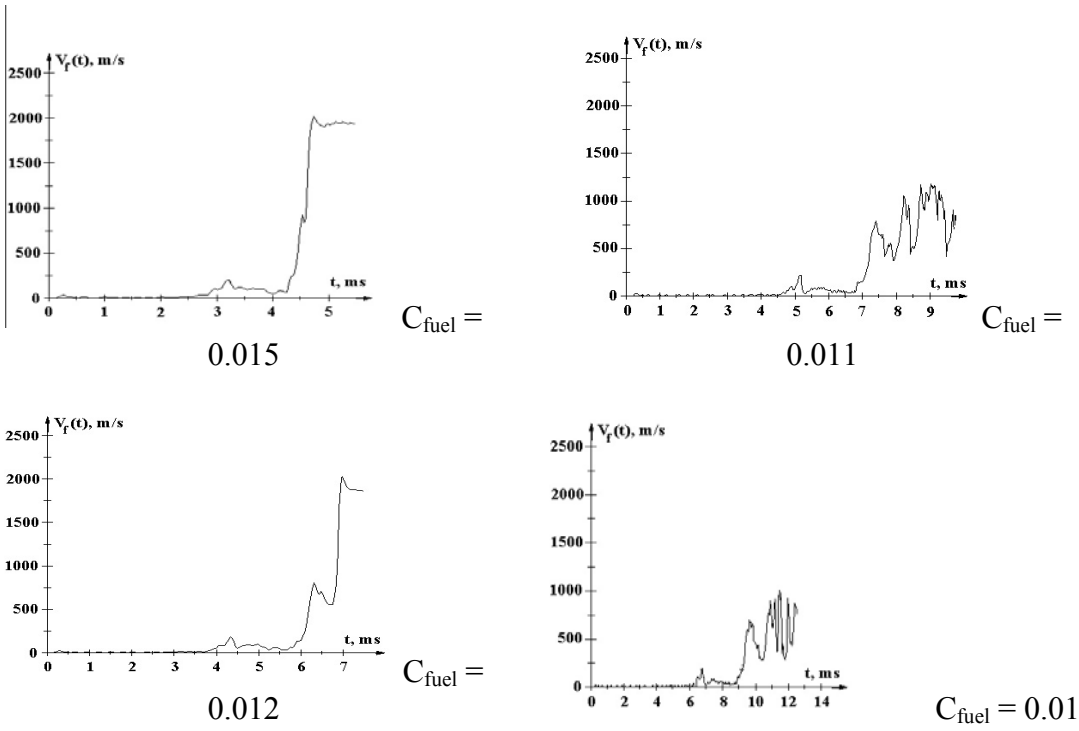

Fig. 7. Reaction front velocity for different fuel concentrations in a two-chamber device.

The role of chambers at the end of the tube

To provide a comparative data we investigated the role of two chambers of a wider cross-section incorporated in the far end of the tube. The tube was identical to that used in previous numerical experiments but symmetrical in respect to 180° rotation (equivalent to ignition performed at the opposite side) (Fig. 5c). Numerical results showed that after ignition in a narrow tube (ignition energy was increased) acceleration of flame zone accompanied by a number of oscillations brought to formation of the detonation wave propagating with mean velocity 1850 m/s. On entering the first chamber decoupling of the shock wave and reaction zone took place and the mean velocity of reaction zone propagation decreased to 200 m/s, then in a narrow bridge flame accelerated up to 400 m/s, and slowed down in the second chamber to 100 m/s. Fig. 8 illustrates reaction front trajectory and velocity variation versus time for the detonation onset and degeneration in a tube with two chambers at the end (fuel concentration was 0.012). Thus similar chambers of wider cross-section incorporated in the end of the detonation tube bring to an arrest of the detonation wave.

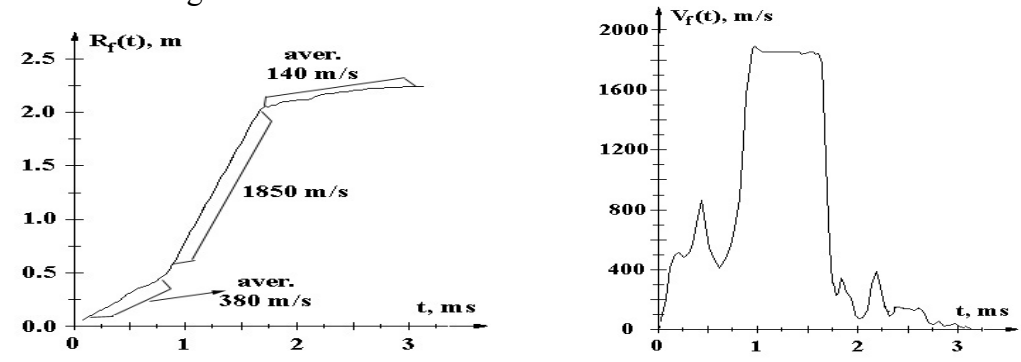

Fig. 8. Reaction front position and velocity for fuel volumetric concentration 0.012

The effect of chambers incorporated in the tube along the whole length

The geometry of the test vessel was the following: the detonation tube 2.95 m length incorporated 20 similar turbulizing chambers uniformly distributed along the axis. The results

showed that for the fuel concentration 0.012 the DDT process did not take place at all. The galloping combustion mode was established characterized by velocity oscillations within the range 80 - 300 m/s, average velocity of flame front 156 m/s. The maps of density and velocity for successive times in the section of the tube incorporating chambers number 6 and 7 are shown in Fig. 8. It is seen that in each chamber combustion passes through similar stages: flame penetration from the tube, expansion and slowing down in the chamber, being pushed into the next tube accelerating due to continuing combustion in the chamber. Reaction zone trajectory and velocity for fuel concentration 0.012 are shown in Fig.9.

The results of numerical experiments show, that increasing the number of turbulizing chambers did not promote the DDT for the present configuration, but just the opposite, it prevented from the onset of detonation and brought to establishing of the galloping combustion mode. The effect took place due to very sharp jumps of the cross-section area in the chambers and periodical slowing the flame down due to its expansion. (In the present numerical experiment the expansion ratio parameter $\beta_{ER} = (S_{chamb} - S_{tube}) / S_{chamb}$ was equal to 0.96.) Why does the increase of the number of chambers up to two promote DDT, while further increase inhibits the process? To answer the question let us regard the flame dynamics in DDT in a two chamber tube (Fig. 10, *a*) keeping in mind that the necessary condition for the DDT is turbulent flame acceleration up to a speed surpassing sonic velocity. Analysis of results shows, that the piston effect of expanding reaction products in the chamber brings to a rapid flame acceleration on entering a narrow tube. After the first chamber flame acquires velocity ~200 m/s, which is less than sonic velocity. After the second chamber flame is pushed into the tube with a velocity 500 - 700 m/s, which surpasses the sonic velocity. Thus further increase of the number of chambers is not necessary as it would not increase chamber exit velocity. Investigations of the sensitivity of self-sustaining combustion modes to expansion ratio parameter show that for small expansion ratios low velocity galloping detonation was established for large expansion ratios self-sustained galloping high speed combustion took place, the transient values of the expansion ratio, which characterize the transition from low velocity detonation to a high speed galloping combustion, increase with the increase of fuel concentration within detonability limits (Fig. 10)

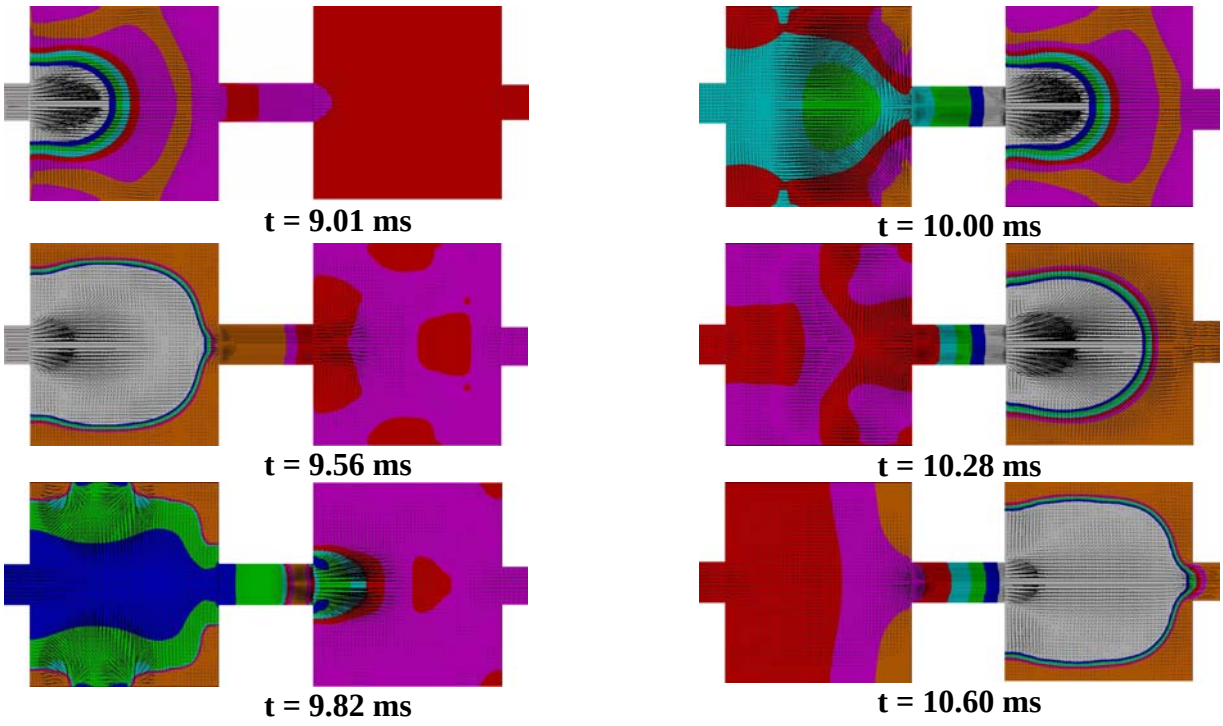

Fig. 8. Density maps in the 6-th – 7-th chambers. Expansion ratio β_{ER}=0.96 , fuel volume concentration 0.012

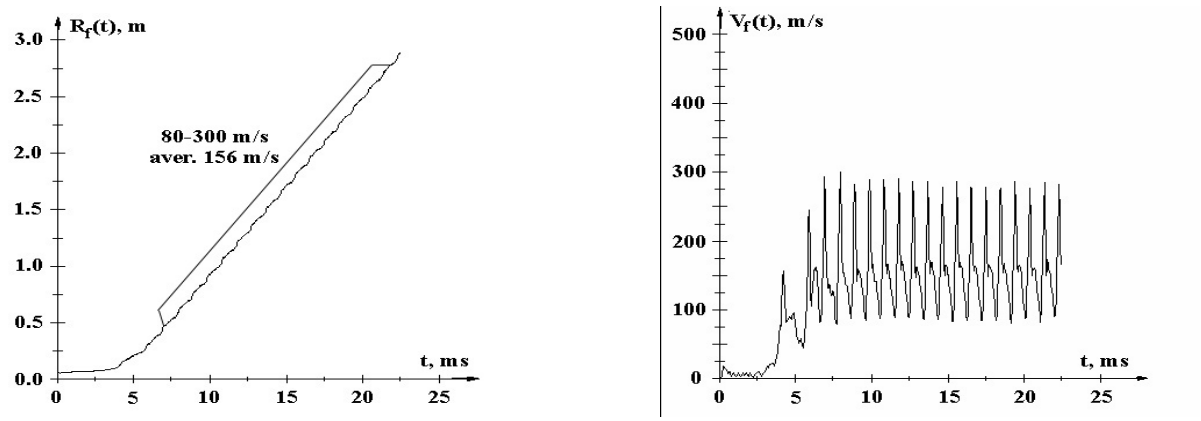

Fig. 9. Reaction front position and velocity in a multi-chamber tube.

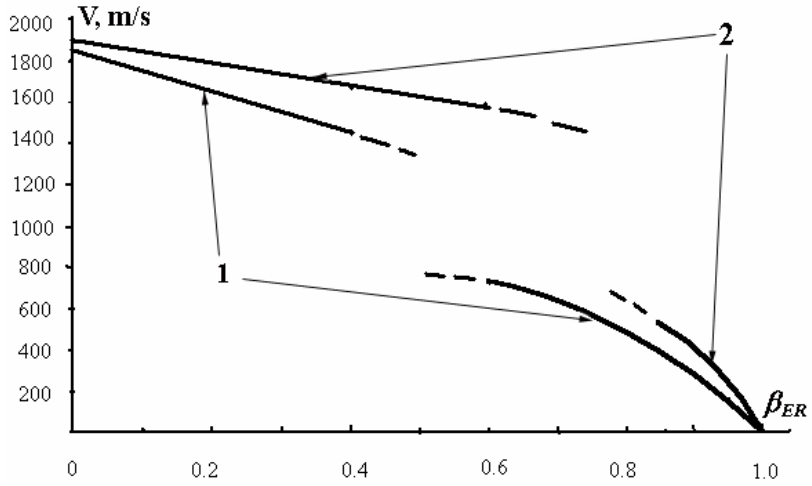

Fig. 10. Mean reaction front velocities in a multi-chamber tube for different expansion ratios:**1** - fuel concentration 0.012; **2** - fuel concentration 0.015.

The influence of mixture temperature on DDT

The influence of temperature on the DDT in gases is one of intriguing issues. The available experimental data on the influence of initial mixture temperature on the DDT process in gases is contradictory. The experiments on DDT in stoicheometric hydrogen-oxygen mixtures in tubes of a constant cross-section at a constant pressure showed the increase of the pre-detonation length with the increase of temperature [36]. On decreasing the content of hydrogen the essential influence of initial mixture temperature on the pre-detonation length was not detected within the temperature range 311K—473K [37]. Investigations of DDT in hydrocarbon fuel-air mixtures [12] in tubes incorporating fore-chambers in the ignition section demonstrated the decrease of pre-detonation length with the increase of initial mixture temperature.

The reason for the results being contradictory stays deep in the physical chemistry of the phenomenon, wherein the increase of initial mixture temperature gives birth to two opposite effects. On one hand, the increase of temperature promotes chemical reactions thus promoting the flame acceleration due to kinetic reasons. On the other hand, transition to the detonation takes place after turbulent flame propagation relative velocity surpasses the speed of sound in gas, which increases with the temperature increase, thus inhibiting the transition process. The decrease of density on increasing the temperature at a constant pressure could be also considered an inhibiting factor. Probably, due to the competition of these opposite effects the available data on the influence of initial mixture temperature on the DDT process in gases is contradictory.

As it has been already mentioned, in stoicheometric hydrogen-oxygen mixtures the increase of temperature brought to the increase of pre-detonation length [35]. Those results testify, that for hydrogen-oxygen mixtures in tubes of constant cross-section the effect of sound velocity increase with the increase of temperature is predominant as compared with the effect of flame speed increase. Thus the combination of both effects retards the DDT.

In our investigations of the DDT in tubes incorporating chambers of a wider cross-section [12, 14, 23] we rely heavily on the role of a piston effect of the expanding reaction products, which penetrate the narrow tube from a wide chamber thus pushing the turbulent flame in the tube assisting it in achieving high velocities surpassing the velocities of sound. Results of numerical modeling (Fig.7) show that on leaving the second chamber flame being pushed into the narrow tube has a velocity surpassing essentially sonic velocity, which is due to gas-dynamics effects. Thus the decrease or increase of sonic velocity in the initial mixture due to temperature variation could hardly influence the criterion to be satisfied. The use of turbulizing fore-chambers neutralizes the negative effect on DDT of sound velocity increase with the increase of temperature. Thus the effect of reduction of chemical induction time with the increase of temperature could turn to be predominant.

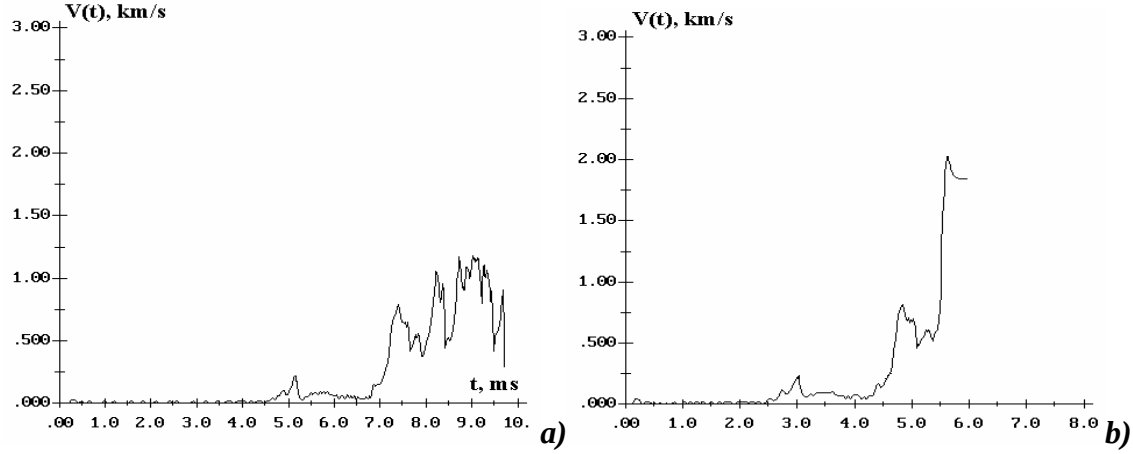

Fig. 11. Flame axial velocity in a two-chamber tube, C_{fuel}=0.011, expansion ratio β_{ER}=0.96, for normal and elevated temperature: ***(a)*** - T_0=300 K; ***(b)*** - T_0=353 K .

Numerical simulations of ignition and flame propagation in lean mixtures (fuel concentration C_{fuel} = 0.011) at an elevated initial temperature (T_0=350 K) showed that the increase of initial temperature of the combustible mixture brings to shortening the pre-detonation length and time. It is seen from Fig. 11, that in case temperature was low (T_0=300K) the onset of detonation did not take place within the length of the test section. High speed galloping combustion occurred for that low fuel concentration. For higher temperature (T_0=353K) DDT took place and a stable detonation mode was achieved via an overdriven regime (Fig. 11, *b*).

Summarizing the above it should be noted, that in detonation tubes with wider fore-chambers in the ignition section the increase of initial mixture temperature promotes DDT and shortens the pre-detonation length. While in tubes of constant cross-section (without any fore-chambers) the effect of initial temperature increase could be the opposite. Thus the role of mixture temperature on detonation initiation needs further deep investigation.

Numerical investigation of gas-droplet interaction in streaming flows.

In order to evaluate the influence of different factors on the rate of droplet evaporation and mixture formation in heterogeneous detonation, which are the key, let us investigate the problem of droplet interaction with the streaming gas flow taking into account mechanical drag, atomization of droplets, non-equilibrium heat and mass transfer. A series of model problems was regarded, in which gas flow and droplet initially had different relative velocities and temperatures, and then relaxation took place. Those model problems are similar to that encountered in shock wave initiation of detonation in combustible dispersed fuel-air mixtures. The two-phase flow becomes strongly non-equilibrium behind the shock wave, because due to mechanical inertia droplets keep their speed practically constant and gas accelerates on passing the shock wave. Besides, due to thermal inertia, temperature inside droplets practically does not change, while gas temperature increases instantaneously behind the shock wave. Due to that

reason gas temperature in all the numerical experiments was assumed to be higher than the boiling temperature for liquid droplets.

The thermophysical properties for gas and droplets were assumed similar for all numerical experiments: ambient pressure $p = 1,013$ bar, temperature $T = 1000\,\mathrm{K}$, gaseous phase – air, liquid – n-decane ($C_{10}H_{22}$). Initial droplet temperature was assumed to be $T = 300\,\mathrm{K}$.

The relaxation processes for droplets of different diameters were regarded. Numbered lines on the successive figures correspond to the following initial diameters of droplets.

1: D_o=1 μm
2: D_o=5 μm
3: D_o=10 μm
4: D_o=50 μm
5: D_o=100 μm
6: D_o=500 μm
7: D_o=1000 μm

Figs. 12-15 illustrate parameters of droplets variation in the process of mechanical and thermal relaxation for the set of numerical experiments assuming initial velocity difference to be equal to 50 m/s. Fig. 12 illustrates velocity relaxation. It is seen that on decreasing initial droplet radius the relaxation process turns to be faster. The decrease of the relaxation time is monotonous. Some curves begin lower than 50 m/s because the relaxation process is too fast for small droplets, and the time scale on the x-axis is logarithmic beginning from a definite small value.

Fig. 13 illustrates droplet diameter variation due to evaporation. It is seen from the figure that evaporation time increases with the increase of initial droplet diameter, but the increase does not take place monotonously: the increase of life time (curves 1, 2, 3, 4) changes for a decrease (curves 4, 5) and then comes back to an increase (curves 5, 6, 7). That testifies the effect of manifestation of different mechanisms depending on the characteristic size of droplets. The breakup of large droplets (Fig. 13) brings to the conditions that behavior of droplets of initial diameter 500 microns and 1000 microns looks after some time necessary for atomization to proceed.

One could distinguish the characteristic time for each droplet being the function of its initial diameter and relative gas velocity.

$$\tau = \frac{v_0}{a_0}, \text{ where } a_0 = \frac{f_d(t=0)}{m_0}. \tag{33}$$

The time being normalized to this value, and droplet diameter being normalized to its initial value allow us to obtain the dependences for relative values.

Fig. 14 illustrates droplet temperature variation. The dynamics of droplet heating is the following. For small droplets (curves 1, 2, 3, 4) in the very beginning the temperature increases due to external heating. On rapid decrease of droplet relative velocity (Fig. 12) evaporation in the stream of gas brings to a decrease of temperature. Then on decreasing droplet radius heat fluxes growth brings to an increase of temperature until the droplet disappears. The first increase of temperature is higher for larger droplets, which relative velocity decreases much slower than for small droplets. Very large droplets follow different scenario: The first increase of their temperature goes as high as up to the critical value. Then evaporation takes place at a critical temperature very rapidly. Arrows with numbers in Fig. 14 indicate the end of droplet life time. That is the reason for a larger droplet (curves 5 in Figs. 13 and 14) to have a shorter life time.

Fig. 15 illustrates droplet temperature variation versus normalized time t/τ. As it is seen from the figure all maxima and minima of temperature correspond to nearly the same normalized

time moments independently on initial droplet radius. The difference between the two scenarios for droplet behavior in the stream of heated air could be clearly distinguished from this figure.

Figs. 16 - 17 present the results of similar numerical experiments, but for higher initial relative velocity: $V_0 = 100 m/s$. The character of the process looks similar: two different scenario for droplet behavior could be distinguished as well. But for the higher relative velocity smaller droplets already reach critical temperature during the first temperature increase (Figs. 18 and 19). Thus curve 4 belongs already to the second group of curves, which corresponds to the second scenario of droplet heating and evaporation. Fragmentation is more essential for higher relative velocity: curves 4, 5, 6, 7 converge in time due to equalizing of droplet radii in fragmentation (Fig. 18).

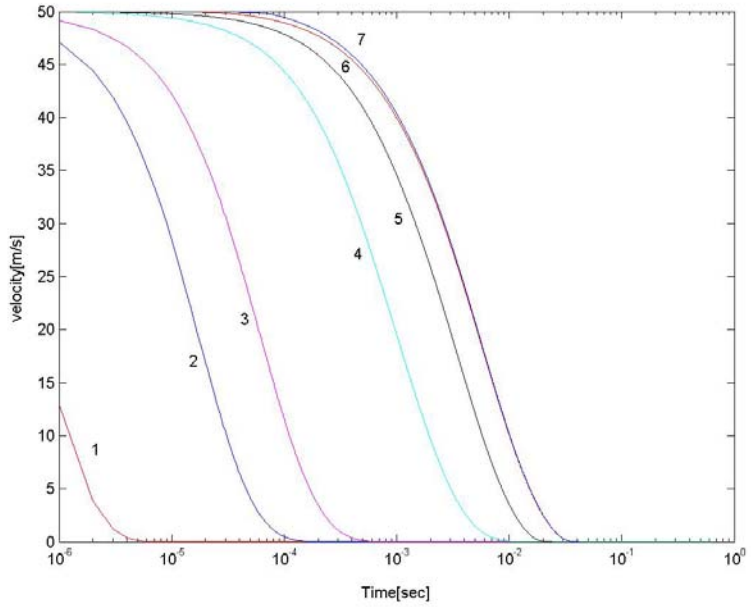

Fig. 12. Velocity relaxation versus time for droplets of different diameters. $V_0 = 50 m/s$, taking into account atomization.

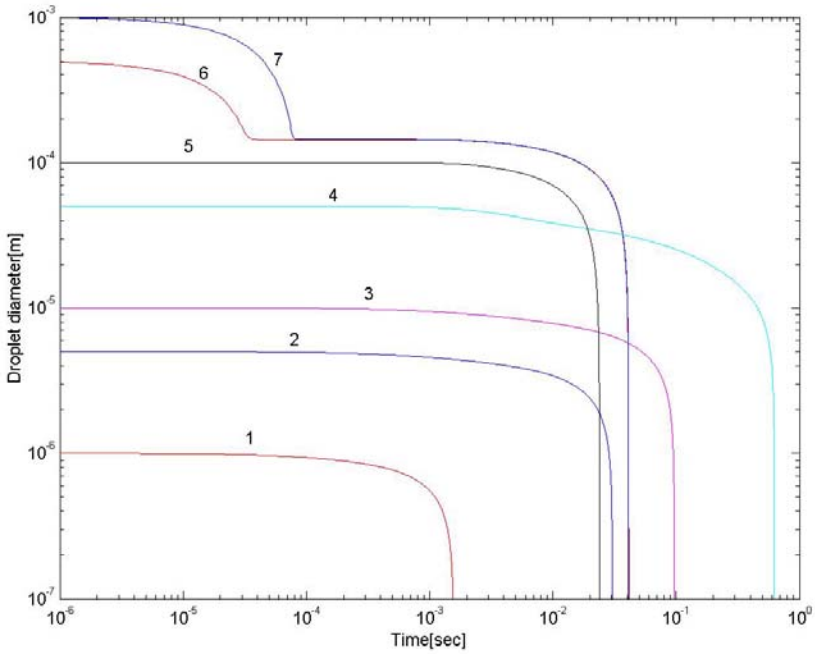

Fig. 13. Droplet diameter variation versus time for droplets of different initial diameters. $V_0 = 50 m/s$, taking into account atomization.

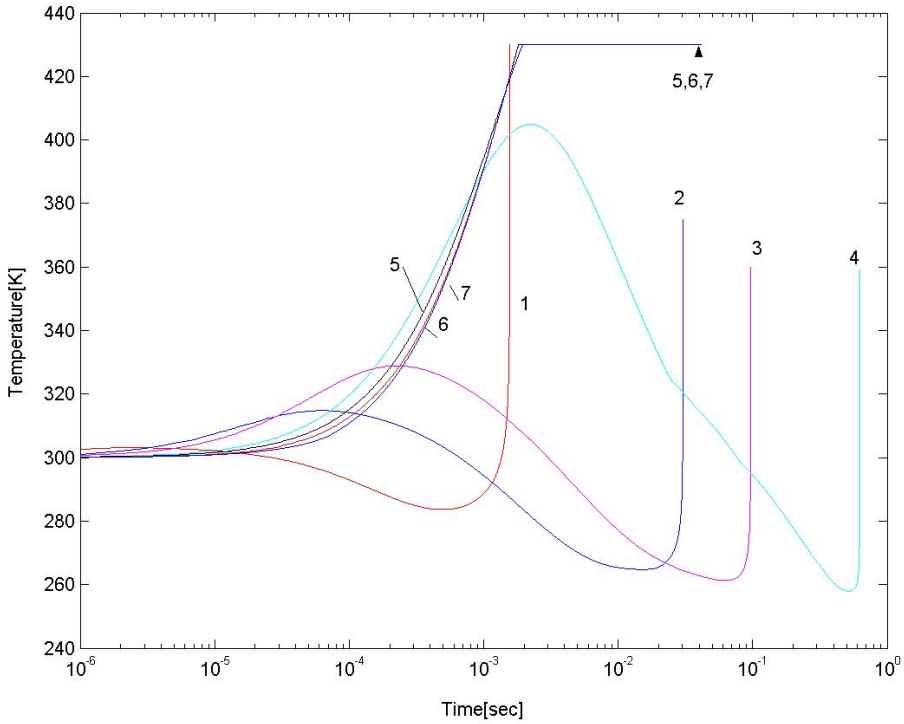

Fig. 14. Mean droplet temperature variation versus time for droplets of different diameters. $V_0 = 50m/s$, taking into account atomization.

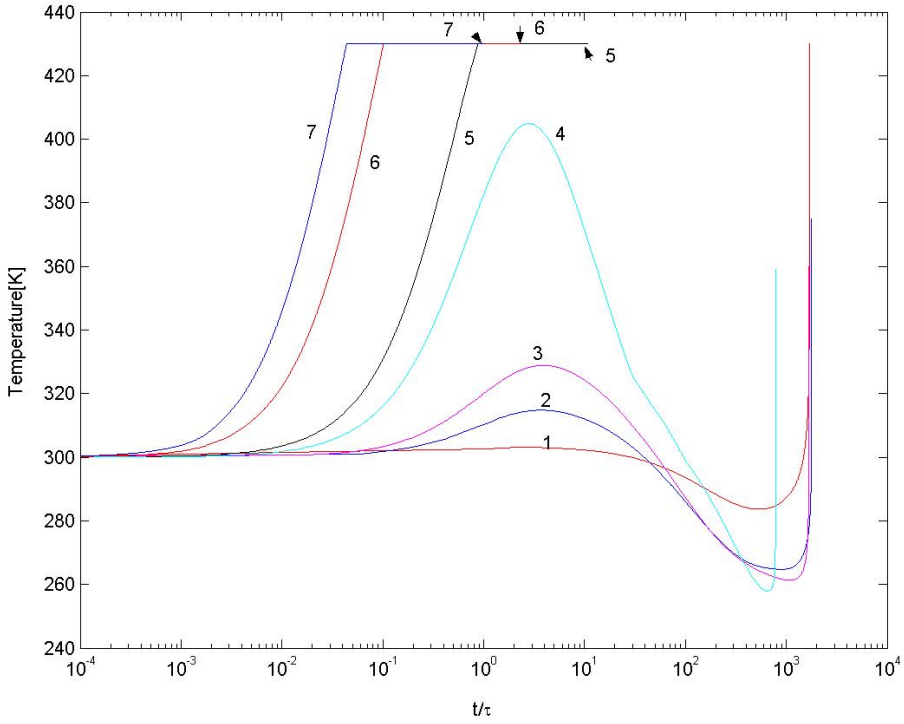

Fig. 15. Mean droplet temperature variation versus normalized time for droplets of different diameters. $V_0 = 50m/s$, taking into account atomization.

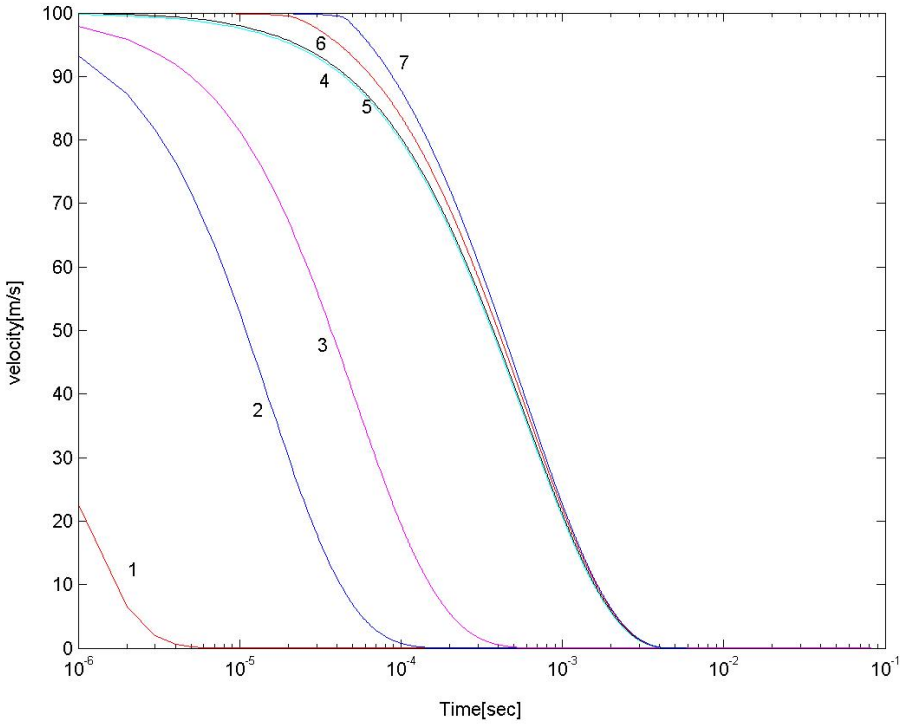

Fig. 16. Velocity relaxation versus time for droplets of different diameters. $V_0 = 100 m/s$, taking into account atomization.

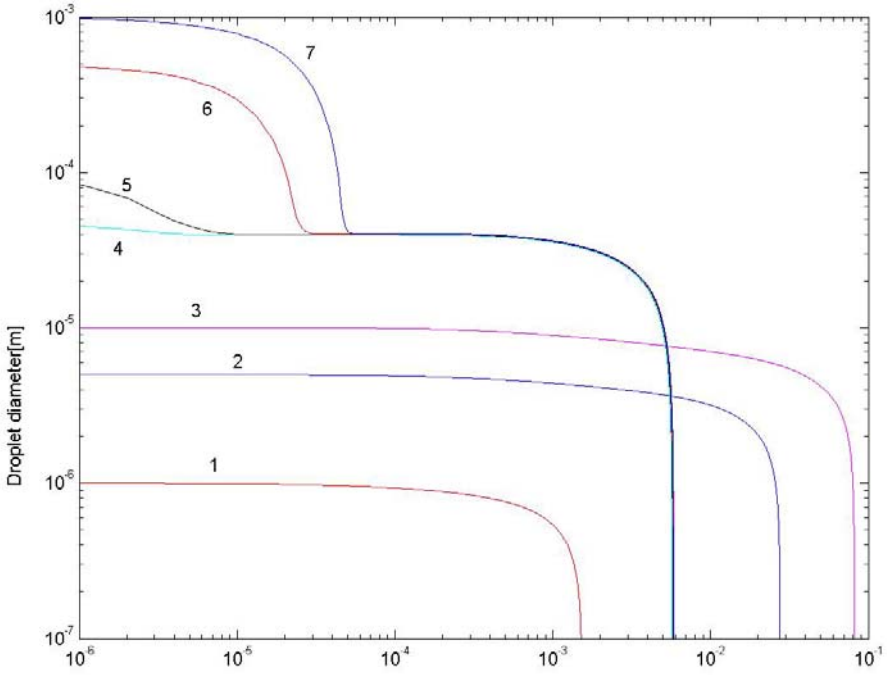

Fig. 17. Droplet diameter variation versus time for droplets of different diameters. $V_0 = 100 m/s$, taking into account atomization.

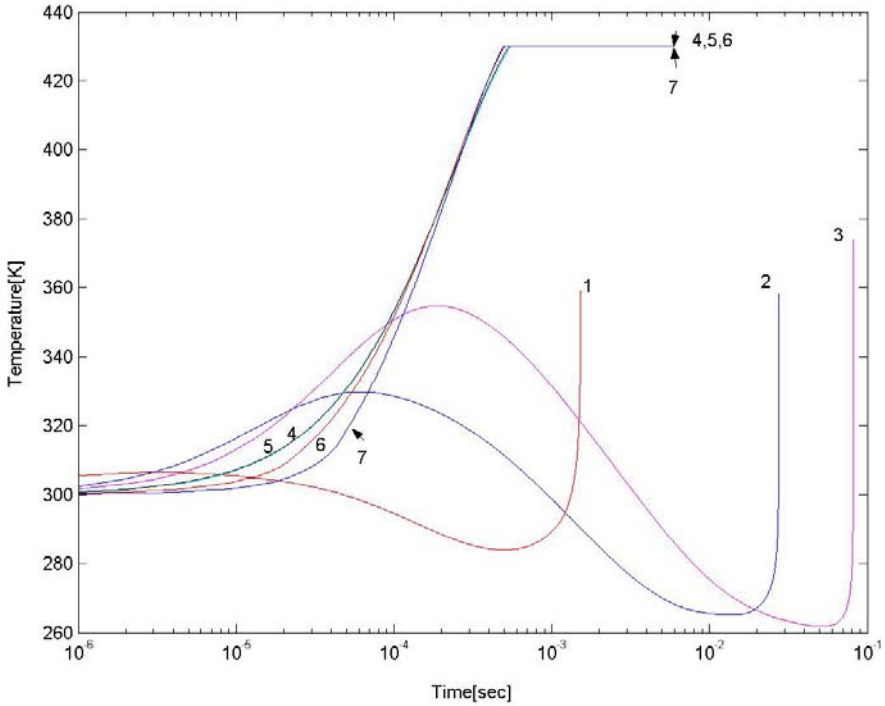

Fig. 18. Mean droplet temperature variation versus time for droplets of different diameters. $V_0 = 100 m/s$, taking into account atomization.

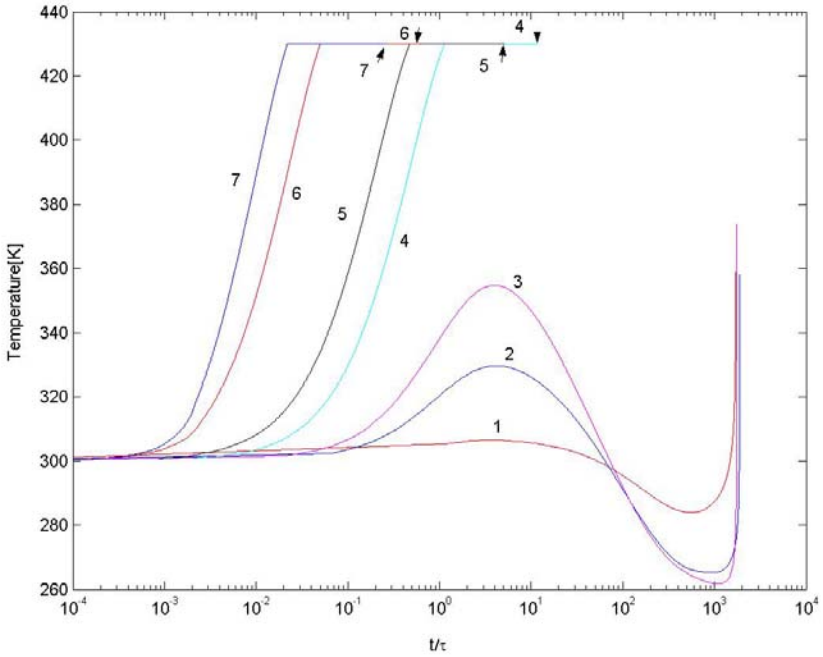

Fig. 19. Mean droplet temperature variation versus time for droplets of different diameters. $V_0 = 100 m/s$, taking into account atomization.

Some model problems for a shock wave interaction with a polydispersed cloud of droplets

Numerical investigations of detonation initiation in dispersed hydrocarbon fuel - air mixtures by shock waves of different intensities were performed. To simulate hydrocarbons the following parameters were taken: ρ = 850 kg/m^3; ΔH = 43 MJ/kg; h_L = 200 kJ/kg; W = 140 kg/kmol. The share of water in hydrocarbon decomposition was assumed to be ζ= 0.2. The mean droplets diameter was assumed 50 μm, minimal diameter – 10 μm, maximal – 100 μm. The

droplets size distribution function was assumed to be a triangular one. The initial droplets volume concentration $\alpha = 0.001$.

The tube diameter was 20 mm, the tube length for numerical modeling was chosen equal to 1 m, but only the zone of 350 mm length was occupied by the polydispersed mixture at ambient pressure temperature 300 K. The rest of the tube was used for a plate shock wave to get formed. The flow was assumed to have the following initial turbulence characteristics: energy k = 0.1 J/kg, the mixing length l = 0.01m, mean velocity $u = 0$. The number of model particles used in calculations was 15000. The scheme of the computational domain is shown in Fig. 20.

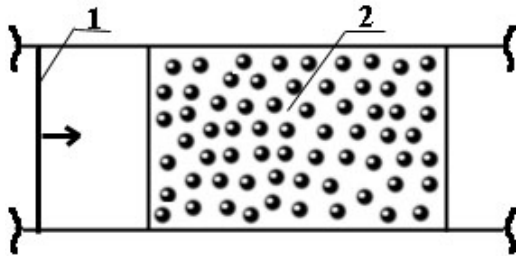

Fig. 20. The scheme of computational domain.

The results show that on entering the dispersed mixture strong attenuation of the initiating shock wave takes place. Behind the shock wave there originates a zone of high concentration of dispersed phase. The profiles of condensed phase concentration behind the shock wave for successive times are shown in Fig.21. The initial volume concentration of condensed phase was uniform starting from $x=x_0$. The zone of increased density of solid particles behind shock waves was first discovered numerically by Korobeinikov [42] and named the ρ-layer. Later, the formation of ρ-layers in dusty gases was confirmed experimentally. The present results show that for liquid droplets ρ-layers are formed as well behind shock waves despite droplets atomization. The density maximum is more close to the shock wave due to atomization and formation of small droplets that could be easier involved into motion by the gas flow. At the same time the shock wave attenuation for atomizing droplets is stronger than for solid particles of the same initial size due to the increase of integral drag forces.

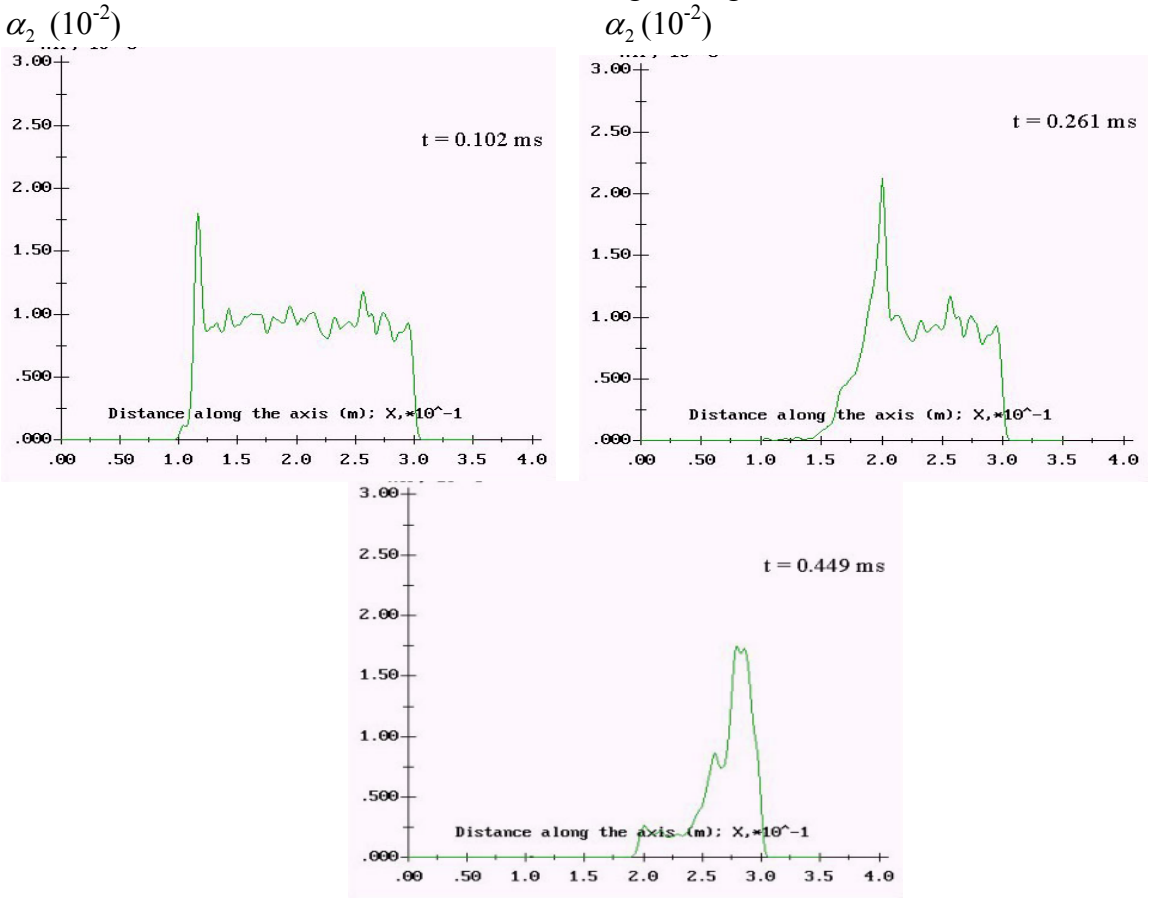

Fig. 21. Condensed phase mean volume share α_2 profiles for successive times in shock wave ignition of dispersed fuel-air mixture. Shock wave propagates from left to right.

Combustion of droplets promotes evaporation thus decreasing the volume fraction of condensed phase behind the shock wave. Nevertheless, the structure of the ρ-layer behind the shock remains the same, but concentration maximums are much lower and essentially more close to the shock wave. The reason for such a behavior of the ρ-layer is the ignition delay. Combustion does not begin simultaneously behind the shock wave, but starts after a some delay. Thus, concentration profiles just behind the shock are similar to that for unburned droplets. Later combustion brings to a rapid decrease of condensed phase concentration. Thus, the combination of the opposite effects shifts the concentration maximum more close to the shock wave.

Energy release in combustion of dispersed mixture decreases the attenuation of the initiating shock wave and can bring in the long run to its acceleration. Fig. 22 illustrates droplets size and temperature distributions in the tube for successive times after the shock wave entered the zone of dispersed mixture. Atomization and heating of small droplets take place behind the shock wave. Atomization is non-uniform in the cross-section of the tube: large droplets are still present near the wall being suspended later into the core, of the shock induced flow. The rate of heating of atomized droplets decreases gradually on penetrating the shock deeper into the dispersed mixture due to a rapid attenuation of the shock wave.

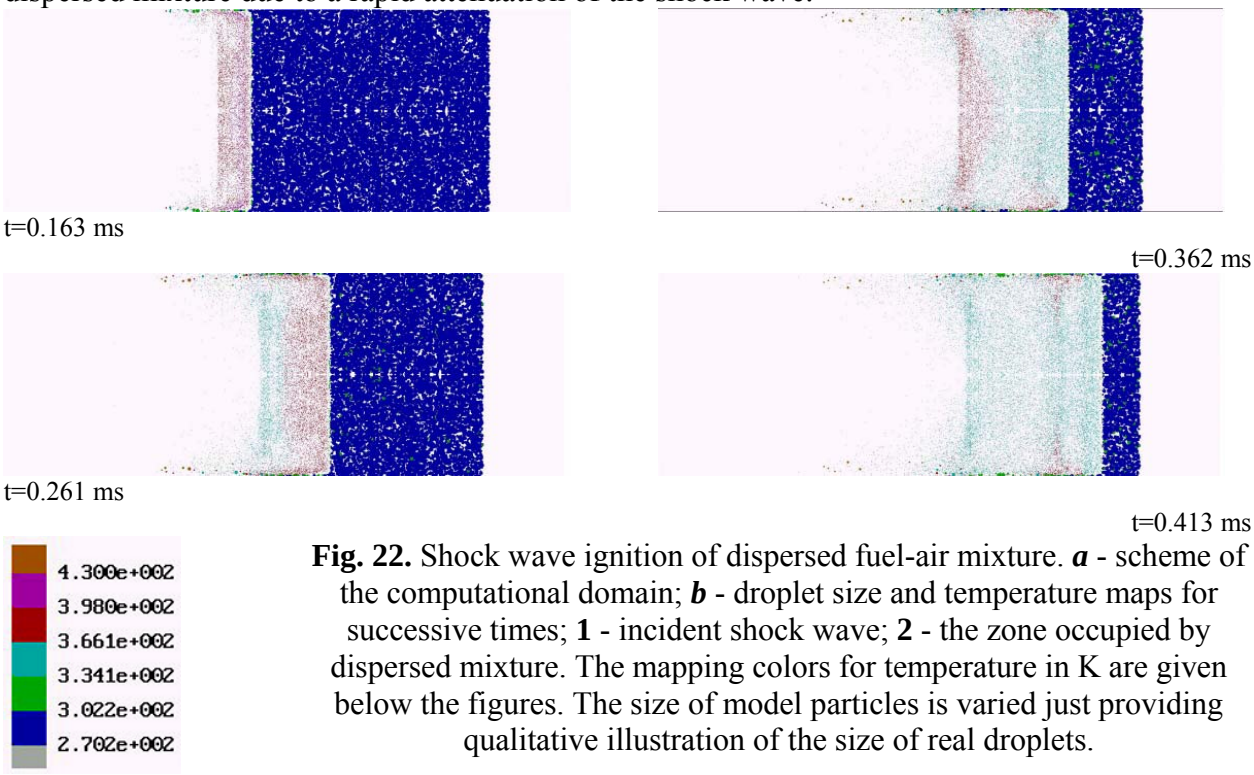

Fig. 22. Shock wave ignition of dispersed fuel-air mixture. ***a*** - scheme of the computational domain; ***b*** - droplet size and temperature maps for successive times; **1** - incident shock wave; **2** - the zone occupied by dispersed mixture. The mapping colors for temperature in K are given below the figures. The size of model particles is varied just providing qualitative illustration of the size of real droplets.

The example illustrated in Fig. 22 shows the onset of the detonation wave in the atomized and pre-heated mixture compressed by the primary shock wave. The detonation wave is characterized by a very narrow reaction zone, wherein most of small droplets burn out.

The cases of deflagration to detonation transition in poly-dispersed gas-droplet mixtures are illustrated in Fig. 23. Mixtures characterized by different droplet size distribution function (left hand side of the Fig. 23) were investigated for comparative purposes. For all the test cases fuel volume ratio was kept constant. The right hand side of the figure illustrates flame velocity variation versus distance. It is evident that the onset of detonation takes place via an overdriven mode after several oscillations of velocity. The droplet size distribution function does not have an essential influence on the predetonation length.

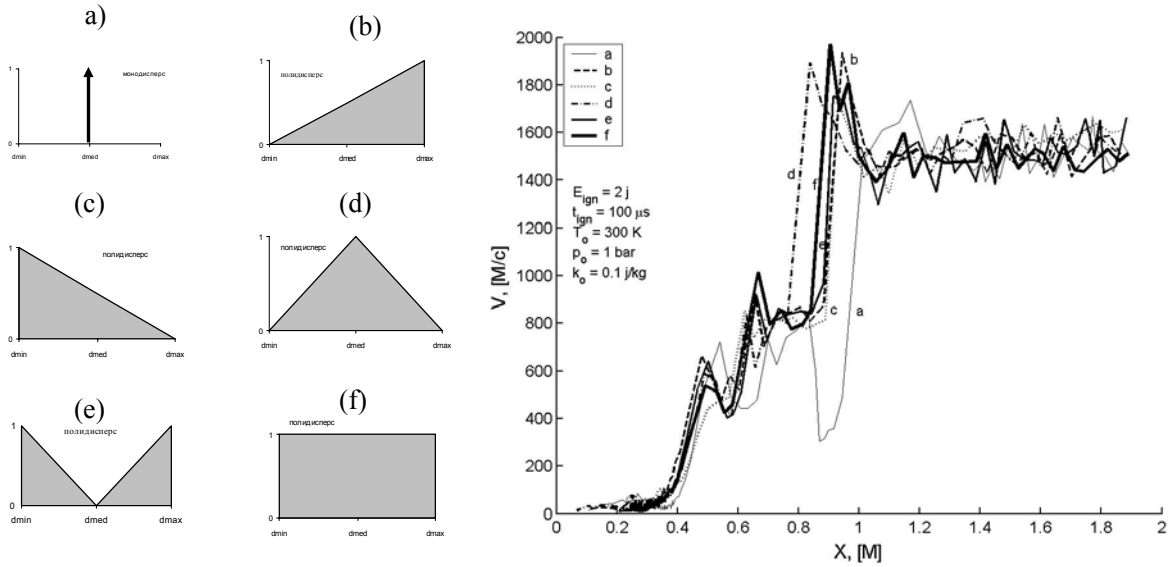

Fig. 23. The effect of droplet size distribution on the onset of detonation in poly-dispersed mixtures.

The Fig. 24 illustrates the dependence of flame velocity in DDT versus time. It is seen from the figure that droplet size distribution function affects the predetonation time. The onset of detonation comes earlier for the case small fraction of droplets is dominating (case *c*), while for the dominating large fraction (case *b*) the onset of detonation comes later. The difference between mono-disperse mixture (case *a*) and uniform droplet distribution versus size (case *f*) is practically negligible.

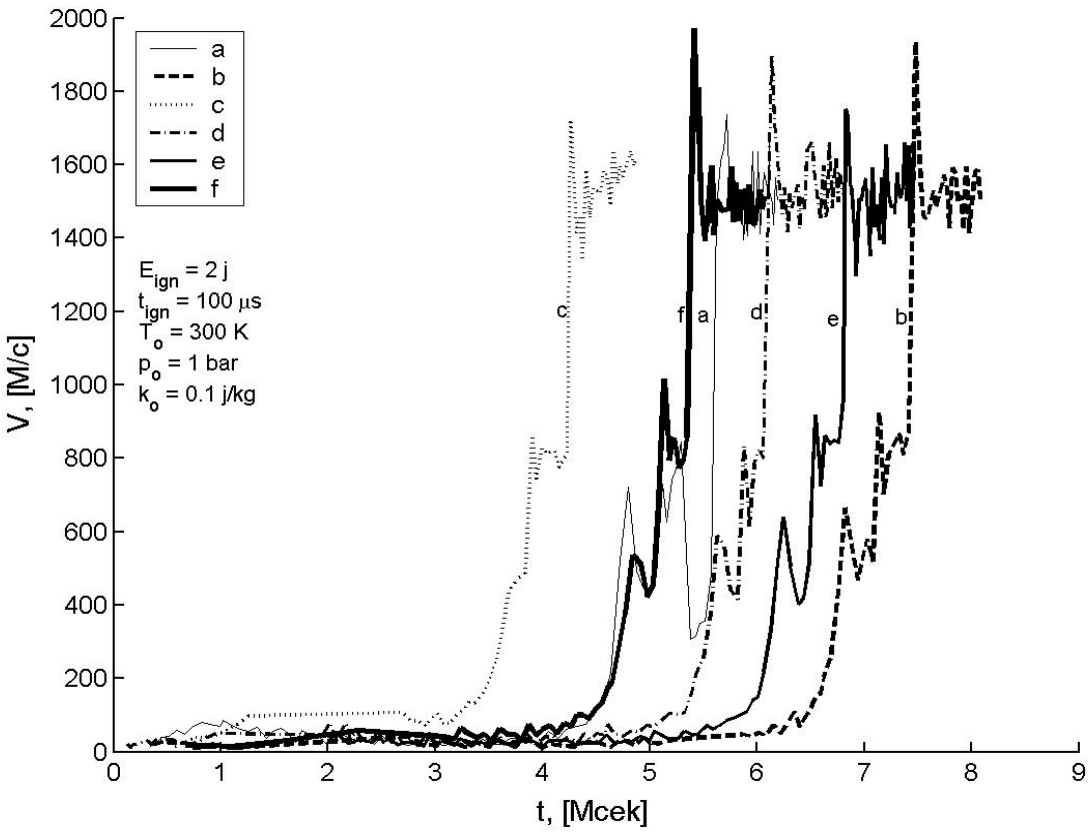

Fig. 24. The effect of droplet size distribution on the onset of detonation in polydispersed mixtures. Velocity versus time diagram.

The developed model made it possible for the first time to investigate the effects of droplets distribution non-uniformity on the DDT in poly-dispersed mixtures.

Conclusions.

The undertaken investigations show that flame propagation velocity is essentially dependent on geometry of the combustion chamber. The presence of wider cavities in the combustion channel brings to a rapid flame acceleration, which could even result in a changing of combustion wave propagation mode from deflagration to detonation.

Depending on geometrical constraints and mixture composition different combustion regimes could be established, such as low velocity combustion, high speed galloping combustion, low velocity detonation, Chapman-Jouget and overdriven detonation modes.

The presence of one or two turbulizing chambers of a wider cross-section in the ignition section shortens the pre-detonation length for hydrocarbon-air gaseous mixtures and makes the onset of detonation more stable.

The increase of the number of similar chambers uniformly distributed along the tube blocks the onset of detonation: galloping highs speed combustion modes were established for large expansion ratios, or low velocity galloping detonations were established for small expansion ratios. Mean reaction front axial velocity grows with the increase of hydrocarbon fuel concentration in the range of 0.010 - 0.015. For expansion ratios within the range 0.4 - 0.6 the increase of fuel content could bring to a change of propagation regime: galloping combustion mode could be changed for the low velocity detonation regime. Transient values of the expansion ratio, which characterize the transition from low velocity detonation to a high speed galloping combustion increase with the increase of fuel concentration within detonability limits.

The increase of the number of turbulizing fore-chambers in the ignition section promotes DDT until flame velocity on leaving the last fore-chamber surpasses sonic velocity. The further increase of the number of chambers inhibits DDT.

The increase of initial mixture temperature in tubes incorporating turbulizing fore-chambers of wider diameter in the ignition section promotes DDT and shortens pre-detonation length, while in tubes without fore-chambers the effect of temperature increase on DDT could be quite the opposite bringing to the increase of pre-detonation length.

Investigations of the detonation initiation in two-phase dispersed mixtures showed that:

- Prior to ignition the process of mixture formation consumes a lot of initiation energy to heat, evaporate and set to motion fuel droplets.
- Investigating the behavior of individual droplets in a heated air flow allowed to distinguish two scenarios for droplet heating and evaporation. Small droplets undergo successively heating, then cooling due to heat losses for evaporation, and then rapid heating till the end of their life time. Larger droplets could directly be heated up to a critical temperature and then evaporate rapidly.
- Atomization of droplets interferes the heating and evaporation scenario.
- On entering the dispersed mixture the shock wave forms behind it a zone of increased concentration of the dispersed phase — the so-called ρ-layer. In combustible dispersed mixture the ρ-layer is thinner than that formed in inert dispersed mixture.
- The onset of detonation in case of a mild ignition of liquid hydrocarbon fuel-air dispersed mixtures at ambient pressures and temperatures comes via an overdriven regime.
- The effect of poly-dispersed character of droplets on the DDT was investigated. The onset of detonation was shown to come earlier for the case small fraction of droplets was dominating (case *c*), while for the dominating large fraction (case *b*) the onset of detonation used to come later. The difference of pre-detonation length and time between mono-disperse mixture (case *a*) and uniform droplet distribution versus size (case *f*) was practically negligible.

By now, initiating of heterogeneous detonation by a strong shock wave is rather well investigated, while the peculiarities of a mild ignition and successive deflagration to detonation transition are not well understood. Thus, it is necessary to concentrate efforts in future research

on peculiarities of control of DDT processes and detonation onset in polydispersed fuel-air mixtures, and reveal the promoting mechanisms.

Acknowledgements.

President of Russian Federation grant (НШ-19.2003.1), Russian Foundation for Basic Research (grant 05-03-32232) and ISTC grant 2992 are acknowledged for financial support.

References

1. Mallard E., Le Chatelier H.L. Compt. Rend. Acad. Sci. Paris, v. 93, (1883) 145.
2. Berthélot M., Vieille P. Compt. Rend. Acad. Sci. Paris, v. 93, (1883) 18.
3. Михельсон В.А. О нормальной скорости воспламененія гремучихъ газовыхъ смѣсей. Учен. Зап. Импер. Моск. ун-та. Отделъ физ.-матем. 1893, вып. 10, стр. 1-92. (Mikhelson V.A. On normal combustion velocity of explosive gaseous mixtures. Imperial Moscow University Scientific Bulletin. Phys. & Math. Ser., 10, (1893) 1-92.)
4. Rankine W.J.M. Phil. Trans. (1870), 277-288.
5. Hugoniot H. Journ. Liouville. v.3, (1887), 477-492; v. 4, (1888), 153-167.
6. Chapman D.L. Phil. Mag. v. 47, (1899) 90.
7. Jouget E.J. Mathematics. 1905, p. 347.
8. Salamandra G.D. On interaction of a flame with a shock wave. In: Physical Gasdynamics, USSR Acad. Sci. Publ., 1959, 163-167.
9. Oppenheim A.K., Urtiew P.A. Experimental observations of the transition to detonation in an explosive gas, Proc. Roy. Soc., A295, (1966) 13.
10. Soloukhin R.I. Methods of measure and main results of experiments in shock tubes. Novosibirsk State University Publ., Novosibirsk. 1969.
11. Oppenheim A. K., Soloukhin R. I. Ann. Rev. Fluid Mech., 5, (1973) 31.
12. Smirnov N.N., Boichenko A.P. Deflagration to detonation transition in gasoline-air mixtures, Combustion, Explosion and Shock Waves, 22, 2, (1986) 65 - 68.
13. Lindstedt R. P., Michels H. J., Deflagration to detonation transition in mixtures of alkane LNG/LPG constituents with O_2 / N_2, Combustion and Flame, 72, 1, (1988) 63 - 72.
14. Smirnov N.N., Tyurnikov M.V. Experimental Investigation of Deflagration to Detonation transition Hydrocarbon-air gaseous mixtures, Combustion and Flame, 100, (1995) 661-668.
15. Zeldovich Ya. B., Librovich V.B., Makhviladze G.M. and Sivashinsky G.I. On the onset of detonation in a non-uniformly pre-heated gas. Sov. J. Applied Mechanics and Technical Physics, 2, (1970) 76.
16. Merzhanov A.G. Combustion and Flame, 10, (1966) 341-348.
17. Borisov A.A. Acta Astronautica, 1, (1974) 909-920.
18. Kailasanath K. and Oran E.S. Ignition of flamelets behind incident shock waves and the transition to detonation. Combustion Science Technology, 34, (1983) 345-362.
19. Zeldovich Ya.B., Gelfand B.E., Tsyganov S.A., Frolov S.M., Polenov A.N. Concentration and temperature non-uniformities of combustible mixture as a reason of pressure waves generation. In: Dynamics of Explosions (A Kuhl et al. Eds.) AIAA Inc., New York, 114, (1988) 99.
20. Smirnov N.N., Demyanov An.Yu., Panfilov I.I. Deflagration to detonation transition, Chemical Physics of Comb. and Expl.: Detonation. USSR Acad. Sci. Publ., 1989, 52-56.
21. Wolanski P., Archivum Combustions, № 3 - 4, (1991) 143 - 149.
22. Smirnov N. N., Panfilov I. I., Deflagration to detonation transition in combustible gas mixtures, Combustion and Flame, v. 101, (1995) 91 - 100.
23. Smirnov N.N., Nikitin V.F., Boichenko A.P., Tyurnikov M.V., Baskakov V.V. Deflagration to detonation transition in gases and its application to pulse detonation devices. In: Gaseous and Heterogeneous Detonations: Science to Applications (G.D.Roy et. al. Eds.) Moscow, ENAS Publ. 1999, pp.65-94.

24. Brown C.J., Thomas G.O. Experimental studies of shock-induced ignition and transition to detonation in ethylene and propane mixtures. Combustion and Flame, 117, (1999) 861-870.
25. Khohlov A.M., Oran E.S. Numerical simulation of detonation initiation in a flame brush: the role of hot spots, Combustion and Flame, 119, (1999) 400-416.
26. Shchelkin K.I., Troshin Ya.K. Gasdynamics of Combustion. USSR Academy Sci. Publ., Moscow. 1963.
27. Knystautas R., Lee J.H.S., Sheperd J.E., Teodorczyk A. Flame acceleration and transition to detonation in benzene-air mixtures. *Combustion and Flame*, 115, (1998) 424-436.
28. Fischer M., Pantow E., Kratzel T. Propagation, decay and re-ignition of detonations in technical structures. In: Gaseous and Heterogeneous Detonations: Science to Applications (G.D.Roy et. al. Eds.) Moscow, ENAS Publ. (1999) pp.197-212.
29. Smirnov N.N., Nikitin V.F., The Influence of Confinement Geometry on Deflagration to Detonation Transition in Gases. J. Phys. IV France, 12, Pr7, (2002) 341-351.
30. Smirnov N.N., Nikitin V.F., Tyurnikov M.V., Boichenko A.P., Legros J.C., Shevtsova V.M. Control of detonation onset in combustible gases. In: High Speed Deflagration and Detonation. (G.D. Roy et al. Eds.) Moscow, Elex-KM Publ., (2001) 3-30.
31. Philip M. Dissertation "Experimentelle und theoretische Untersuchungen zum Stabilitatsverhalten von Drallflammen mit zentraler Ruckstromzone". Karlsruhe University. 1991.
32. Pironneau O. and Mohammadi B. Analysis of the K-Epsilon turbulence model. Masson Editeur, Paris, 1994.
33. Oran E.S., Boris J.P., Numerical simulation of reactive flow. Elsevier, New York. 1987.
34. Smirnov N.N., Nikitin V.F. Unsteady-state turbulent diffusive combustion in confined volumes. Combustion and Flame, 111, (1997) 222 - 256.
35. Anderson D.A., Tannehill J.C., Pletcher R.H., Computational Fluid Mechanics and Heat Transfer. Hemisphere Publ. Co. 1984.
36. Laffitte P. Influence of temperature on the formation of explosive waves. Comp. Rendu, 186, (1928) 951.
37. Bollinger L.E., Fong M.C., Edse R. Experimental measurement and theoretical analysis of detonation induction distance. ARSJ, 31, (1961) 588.
38. Smirnov N.N., V.F. Nikitin, J.C. Legros, *Combust. Flame*, **123,** (1/2), (2000), 46 – 67.
39. Smirnov N.N., V.F. Nikitin, A.V. Kulchitskiy, J.C. Legros, V.M. Shevtsova in G.D.Roy, P.J.Strikowski (Eds.) *Proc. Thirteenth ONR Propulsion meeting,* Univ. of Minnesota, Minneapolis, 2000, p. 213-232.
40. Smirnov N.N., Zverev I.N. *Heterogeneous combustion*, Moscow University Publishers, Moscow, 1992, 446 p.
41. Azzopardi B.J., G.F. Hewitt, *Multiphase Sci.&Tech*., 9, (1997), 109-204.
42. Korobeinikov V.P., *Archivum Combustionis,* 9, (¼), (1989), 149-152.
43. Smirnov N.N., *Int.J.Heat Mass Transfer,* 1988, vol. 31, No 4, pp. 779--793.